ARTICLE IN PRESS

Morphology-dependent phase transformation of γ-Al$_2$O$_3$

Jaekyoung Lee [a], Himchan Jeon [a], Dong Gun Oh [a], Janos Szanyi [b], Ja Hun Kwak [a,*]

[a] Department of Chemical Engineering, School of Energy and Chemical Engineering, UNIST, 100 Banyeon-Ri, Ulsan 689-798, Republic of Korea
[b] Institute for Integrated Catalysis, Pacific Northwest National Laboratory, Richland, WA 99352, USA

ARTICLE INFO

ABSTRACT

The phase transformations of platelet- and rod-shaped γ-Al$_2$O$_3$ were investigated and compared to that of a commercial sample by XRD, BET surface area measurements, transmission electron microscopy (TEM), solid state ^{27}Al-NMR, and ethanol temperature programmed desorption (TPD) after sequential annealing in air up to 1100 °C. After annealing at 1100 °C, commercial γ-Al$_2$O$_3$ mostly transformed into α-Al$_2$O$_3$ with drastic surface area reduction (from 200 m^2/g to 25 m^2/g). Interestingly, platelet- and rod-shaped γ-Al$_2$O$_3$ which showed exactly the same XRD patterns transformed into different phases upon the high temperature calcinations. Platelet-shaped γ-Al$_2$O$_3$ transformed into θ-phase while the rod-shaped γ-Al$_2$O$_3$ transformed into the δ-phase and not to the α-polymorph. Both platelet- and rod-shaped aluminas retained significantly higher surface area (∼60 m^2/g) than the commercial one after the same treatment at 1100 °C. These results suggest that the phase transformation in γ-Al$_2$O$_3$ is strongly affected by not only the crystal structure of the starting material, but its morphology as well. Ethanol TPD from platelet- and rod-shaped alumina after 1100 °C annealing, showed significantly different desorption profiles which suggest different surface characteristics even though they had almost the same surface areas. These different phase transformations were also supported by solid state ^{27}Al-NMR. After 1100 °C annealing commercial alumina showed the presence of mostly octahedral Al^{3+} ions, but the other two samples displayed even higher number of tetrahedral Al^{3+} ions than the initial γ-Al$_2$O$_3$. Morphological changes were also confirmed by TEM. All these results consistently suggest the morphology-dependent phase transformations of γ-Al$_2$O$_3$ and the improved thermal stability of platelet- and rod-shaped γ-Al$_2$O$_3$ in comparison to a commercial γ-Al$_2$O$_3$.

© 2015 Elsevier B.V. All rights reserved.

1. Introduction

γ-Al$_2$O$_3$ is one of the most important catalytic materials and widely used both as an active catalyst and as a support for catalytically active phases. Due to its high surface area and thermal stability, γ-Al$_2$O$_3$ is intensely used in many chemical processes from petroleum refining to automobile emission control catalysis. It is well known that γ-Al$_2$O$_3$ is one of the metastable transition structural polymorphs formed by thermal decomposition of boehmite (AlOOH) [1–3]. Upon high temperature treatment, the γ-Al$_2$O$_3$ phase transforms through metastable δ- and θ-phases to α-Al$_2$O$_3$, the thermodynamically stable polymorph [1–3]. These phase transformations directly affect both the surface area and the number of active sites, which are critically important for practical applications. For these reasons, considerable research efforts

have been focused on to understand the mechanisms of the thermal phase transformation and possible stabilization of γ-Al$_2$O$_3$ [4–14].

It is well known that oxide additives, e.g., lanthanum oxide and barium oxide, improve the thermal stability of γ-Al$_2$O$_3$ [11,13,14]. Other oxides are also reported to be effective for the stabilization of γ-Al$_2$O$_3$ at high temperature [15,16]. Recently, we reported that penta-coordinated Al^{3+} ions, formed on the (1 0 0) facets of the alumina crystallites, play a crucial role in the phase transition of γ-Al$_2$O$_3$ into the θ-phase [17]. We have shown that when penta-coordinate Al^{3+} sites were eliminated by oxide additives, the thermal stability of the γ-phase increased significantly. We have also shown that although the XRD pattern of a calcined Al$_2$O$_3$ sample suggested pure γ-phase, the surface exhibited chemical properties consistent with that of the θ-phase using surface sensitive ethanol TPD [18]. These results strongly suggested that the phase transition was initiated by surface processes on specific crystal facets of γ-Al$_2$O$_3$.

Although the alumina surface is critical for the phase transformation, it is hard to characterize the commercial alumina because of their structural complexities and small domain sizes. Recent

advances in nanotechnology allow us to prepare nano-faceted Al_2O_3 with systematic variations in their morphologies [2,19–25]. Thus, the prepared crystallites have different relative ratios of specific facets allowing systematic studies aimed at finding correlations between phase transformations of γ-Al_2O_3 and crystallite morphologies that otherwise would be very difficult with commercial γ-Al_2O_3. These information will be very useful for potential development of thermally stable γ-Al_2O_3 without any surface modifier such as La, Ba, etc., that can affect the catalytic properties [11,13–16,26–29].

In this study, we investigated the phase transformation of platelet- and rod-shaped γ-Al_2O_3 [21] by XRD, BET, ethanol TPD, solid state ^{27}Al-NMR and HR-TEM after sequential calcinations in air up to 1100 °C. After 1100 °C treatment, commercial γ-Al_2O_3 transformed to α-Al_2O_3 while platelet transformed to the θ-phase and rod transformed to the δ-phase. Furthermore, platelet- and rod-shaped alumina showed much higher surface areas (60 m^2/g) than commercial γ-Al_2O_3 (25 m^2/g) after 1100 °C annealing. In addition to higher thermal stabilities of platelet- and rod-shaped aluminas in comparison to commercial alumina, they showed different catalytic properties after 1100 °C calcination. These results consistently suggest the morphology-dependent phase transformations of γ-Al_2O_3 and improved thermal stabilities of platelet- and rod-shaped Al_2O_3 in comparison to a commercial γ-Al_2O_3.

2. Experimental

Platelet- and rod-shaped γ-Al_2O_3 samples used for this study were synthesized based on a previous report [21]. Typical synthetic procedure for rod-shaped γ-AlOOH was as follows. First, $Al(NO_3)_3 \cdot 9H_2O$ (24.9 g) was dissolved in distilled water (400 ml) to form a transparent solution. Then, hydrazine monohydrate ($N_2H_4 \cdot H_2O$, 10.8 g) was dropped into the solution, giving rise to a milky precipitate at pH = ~5. The resultant reaction mixture was transferred into a 500 ml Teflon-lined autoclave, which was then sealed and kept in the electric oven at 200 °C. After 12 h, the resultant precipitates were collected by centrifugation, repeatedly washed by DI water and isopropyl alcohol, and dried in air at 100 °C for 12 h. Platelet γ-AlOOH were also synthesized using the same procedure except that the initial pH value of the reaction mixture was controlled to 9–10. The as-prepared-AlOOH samples were calcined in a muffle furnace at 600 °C for 3 h, resulting in the platelet- and rod-shaped γ-Al_2O_3.

Three γ-Al_2O_3 samples, commercial (Puralox SBA-200 from Sasol), platelet- and rod-shaped alumina were used in this work. Both platelets and rods were synthesized by the synthesis protocols described above. Each γ-Al_2O_3 samples (0.5 g) were calcined in a muffle furnace in air atmosphere simultaneously at specific temperatures for 3 h. The annealing temperature was increased stepwise from 600 °C to 1100 °C in 100 °C intervals.

After the synthesis, X-ray diffraction (XRD) analysis was carried out to confirm the phase of the alumina. XRD patterns were obtained on a Bruker D8 Advance using Cu Kα radiation (λ = 1.5406 Å) in step mode between 2θ values of 5° and 75°, with a step size of 0.05°/s. The specific surface areas of the alumina samples were determined by the BET method using an automated adsorption instrument (ASAP2420). Prior to N_2 adsorption, the samples were treated in dry N_2 flow at 150 °C for 4 h.

To characterize surface properties of the thermally treated alumina samples, ethanol TPD experiments were carried out using the same experimental procedures as described in our previous report [30]. Prior to ethanol TPD experiments, 0.05 g of pre-treated alumina was annealed again at 500 °C for 1 h under He flow (1.0 ml/s). After calcination, the sample was cooled down to room temperature (23 °C), and ethanol adsorption was carried out for 30 min

using a 2.0% ethanol/He gas mixture (1.0 ml/s), followed by a He purge for 30 min in order to remove weakly-bound ethanol molecules. After stabilization of the flame ionization detector (FID) signal of an Agilent 7820A gas chromatograph (GC), a TPD experiment was carried out in flowing He (1.0 ml/s) with a heating rate of 10 °C/min, and the reactor outlet flowing directly to the FID (i.e., no GC column separation).

All solid state ^{27}Al-NMR experiments were performed at room temperature on a Varian VNMRS 600 MHz FT-NMR spectrometer, operating at a magnetic field of 14.4 T. The corresponding ^{27}Al Larmor frequency was 156.299 MHz. All the spectra were acquired at a sample spinning rate of 25 kHz, using a 1.6-mm pencil-type MAS probe. Each spectrum was acquired using a total of 2000 scans with a recycle delay time of 1 s. All spectra were externally referenced (i.e., the 0 ppm position) to a 1 M $Al(NO_3)_3$ aqueous solution. We normalized the ^{27}Al MAS spectra with the same total NMR peak area for the ease of comparison.

Transmission electron microscopy (TEM) images were taken with a JEM-2100 unit operated at 200 kV. A TEM samples were prepared by dropping alumina particles onto a glass slide, and the particles were carefully ground between two glass slides. By sliding the carbon coated Cu grid onto the glass slide, ground particles were transferred onto the Cu grid.

Steady-state ethanol dehydration reaction was performed in a quartz flow reactor using 0.01 g samples supported by quartz wool. Samples were treated in flowing 20% O_2/He at 500 °C for 1 h. The carrier gas (He) was passed through a bubbler containing ethanol (99.5%, Sigma–Aldrich) kept at 23 °C and ambient pressure. The ethanol concentration (2%) was controlled by relative He flow rate (total flow rate of He was 1.0 ml/s). The outlet gases were analyzed by a GC (Agilent 7820A) using a HP-FFAP column and FID. Catalytic activities were evaluated under conditions where ethanol conversion was kept below 10%.

3. Results and discussion

We synthesized platelet- and rod-shaped aluminas using the synthesis procedure shown in Fig. 1(a). After hydrothermal treatment at 200 °C, platelet- and rod-shaped boehmite (AlOOH) phases were confirmed by XRD (γ-AlOOH, JCPDS 21-1307), which are shown in Fig. 1(b). Platelet- and rod-shaped boehmites showed identical XRD patterns, but morphological differences were confirmed by TEM analysis discussed later. After calcination at 600 °C, both platelet- and rod-shaped boehmites transformed to γ-Al_2O_3 that was also confirmed by XRD patterns shown in Fig. 1(c). The obtained XRD patterns are consistent with previously reported XRD patterns of γ-Al_2O_3 and also commercial γ-Al_2O_3 (Puralox SBA-200) [31].

We need to point out here that the synthesis protocols used in this study for the preparation of the rod and platelet shaped alumina samples and the subsequently extensive rinsing with water and isopropyl alcohol ensured that no alkali impurities were left in the alumina samples. It has been well documented that impurities such as alkali metals (e.g., Na^+) can substantially modify the thermal stabilities of γ-Al_2O_3 and also influence its phase transformations [11,13,14,26–29].

Morphologies of the synthesized alumina samples were confirmed by TEM analysis (Fig. 2). Panels (a) and (b) show as-synthesized boehmites of typical platelet with a rhombus shape and rod-shaped morphologies. After calcination at 600 °C, boehmites were converted to γ-alumina which shows the same platelet- and rod-shaped morphologies, as shown in Fig. 2(d) and (e) [32]. Commercial γ-alumina, shown in Fig. 2(c), exhibits a morphology of agglomerated particles with irregular shapes. In Fig. 2(d), γ-alumina particles formed from platelet boehmites
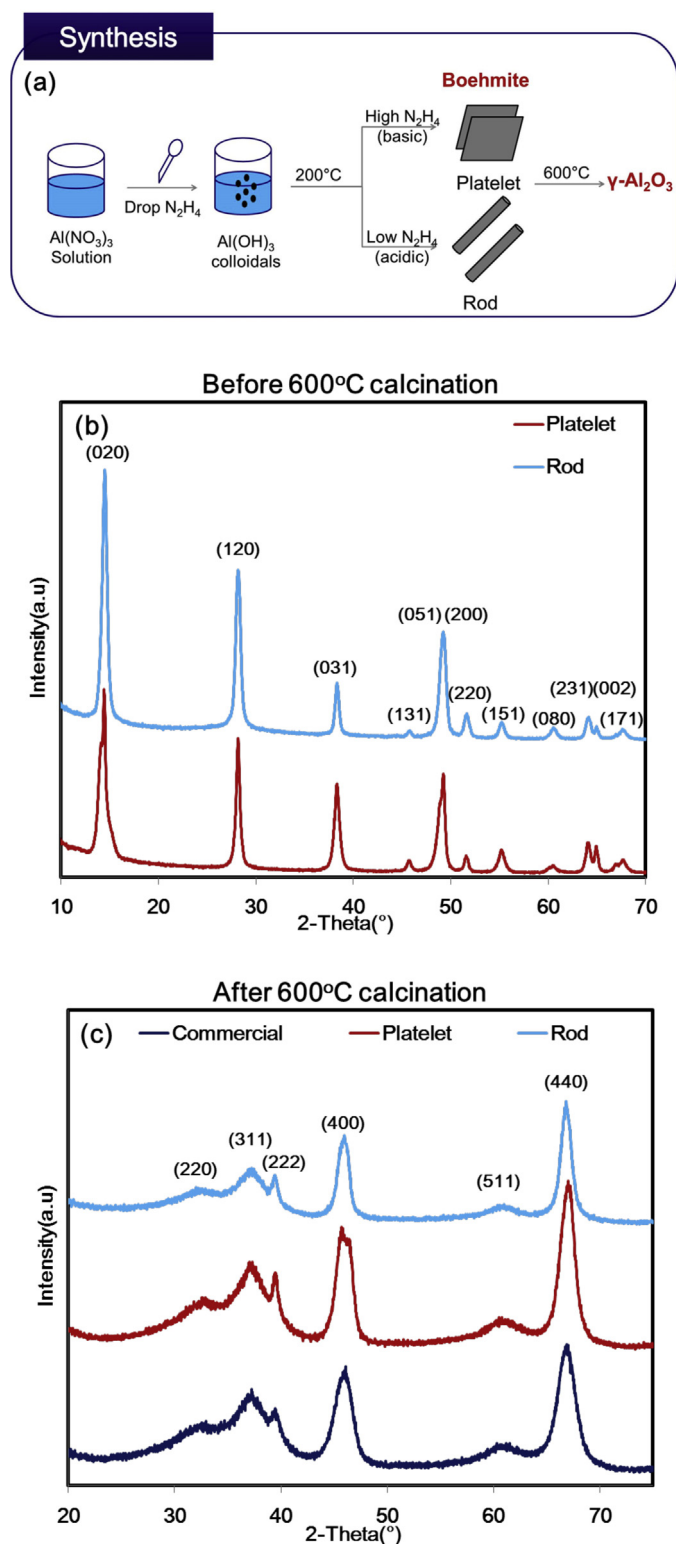
Fig. 1. (a) Overall synthetic procedures for γ-Al$_2$O$_3$ platelets and rods. (b) XRD patterns for synthesized aluminas (platelet and rods) before 600 °C calcination. (c) XRD patterns for commercial alumina (Puralox SBA-200) and synthesized aluminas after 600 °C calcination.

maintained their morphologies of thin platelets of a rhombus shape with short diagonal distance in the plane of 30–70 nm and thickness of 10–20 nm. Some hexagonal-shaped platelet aluminas were also observed. Rod-shaped γ-alumina of 70–180 nm length was observed in Fig. 2(e). The results of XRD and TEM analyses

confirm that all three starting aluminas in this work have γ-phase but very different morphologies.

To investigate the phase transformation of γ-Al$_2$O$_3$ with different morphologies, we heat treated the commercial, platelet- and rod-shaped γ-alumina samples from 600 °C to 1100 °C in air and the obtained aluminas were characterized by BET, XRD, HR-TEM, solid state ^{27}Al-NMR and ethanol TPD.

The effects of heat treatment on the external surface area of alumina were confirmed by the BET method and the results are summarized in Fig. 3. The initial surface area for commercial γ-Al$_2$O$_3$ was 184 m^2/g. Surface areas of the platelet- and rod-shaped γ-Al$_2$O$_3$ were 86 m^2/g and 111 m^2/g, respectively. Those significantly lower surface areas are the consequence of the relatively large crystallite sizes of the synthesized γ-Al$_2$O$_3$ materials in comparison to the commercial one. Rod-shaped alumina showed higher surface area than platelet alumina. With increasing calcination temperature (3 h at each temperature) the surface areas of the γ-Al$_2$O$_3$ samples decreased gradually. Commercial, platelet and rod aluminas all showed similar trend in surface area variation with annealing temperature.

In the 1000–1100 °C temperature ranges the surface areas changed significantly. Commercial γ-Al$_2$O$_3$ showed a drastic surface area decrease to 25 m^2/g after the calcination at 1100 °C. On the other hand, platelet- and rod-shaped aluminas did not show sudden decreases of their surface areas. Initially, commercial alumina had higher surface area than platelet- and rod-shaped ones, while after high temperature calcinations the platelet- and rod-shaped aluminas showed much higher surface areas than the commercial one (platelet – 62 m^2/g, rod – 67 m^2/g and commercial – 25 m^2/g). The severe surface area reduction in the commercial alumina was related to the phase transformation from γ into α which will be discussed by other characterizations later. Interestingly, the platelet- and rod-shaped aluminas did not transform to α-Al$_2$O$_3$ like the commercial sample did, even after 1100 °C calcination. The higher surface areas retained in platelet- and rod-shaped aluminas after 1100 °C calcination suggest better thermal stabilities of these materials in comparison to the commercial γ-Al$_2$O$_3$ studied here.

X-ray diffraction patterns for the three transition γ-Al$_2$O$_3$ samples after 3 h calcinations at the specific temperatures are shown in Fig. 4. These results clearly reveal that, although all the starting aluminas exhibited identical XRD patterns characteristic of the γ-Al$_2$O$_3$ phase as shown in Fig. 2(c), the phase transformations of different alumina samples were dependent on their initial morphologies. XRD patterns obtained from samples calcined from 600 °C to 800 °C showed no apparent deviation from the γ-Al$_2$O$_3$ pattern (only 600 °C patterns shown here). However, XRD patterns collected after calcinations above 900 °C demonstrated notable phase transformations of the alumina samples and, interestingly, showed different patterns depending on their initial morphologies.

After 900 °C calcination of the commercial alumina, phase transformation to δ-Al$_2$O$_3$ was detected (Fig. 4(a)), as the XRD pattern was consistent with that previously reported for δ-Al$_2$O$_3$ (JCPDS no. 47-1770) [31]. Then new diffraction peaks at 2θ values of 31.8°, 32.9°, 51.1°, and 60.3° increased after 1000 °C calcination, indicating the development of the θ-Al$_2$O$_3$ phase [31]. In addition, small sharp peaks were observed at 2θ values of 25.7°, 43.4°, and 57.6°, characteristic of the α-Al$_2$O$_3$ phase (JCPDS no. 010-0173). After 1100 °C treatment, the XRD pattern of the commercial γ-Al$_2$O$_3$ sample was dominated by diffraction peaks of α-Al$_2$O$_3$ (intensity in Fig. 4(a) was reduced by 1/4) while a small portion of θ-Al$_2$O$_3$ phase was also detected. The phase transformation of commercial γ-alumina to α-alumina is consistent with the drastic surface area reduction shown in Fig. 3.

Phase transformation behavior of the platelet shaped γ-alumina was somewhat different from the commercial one as shown in
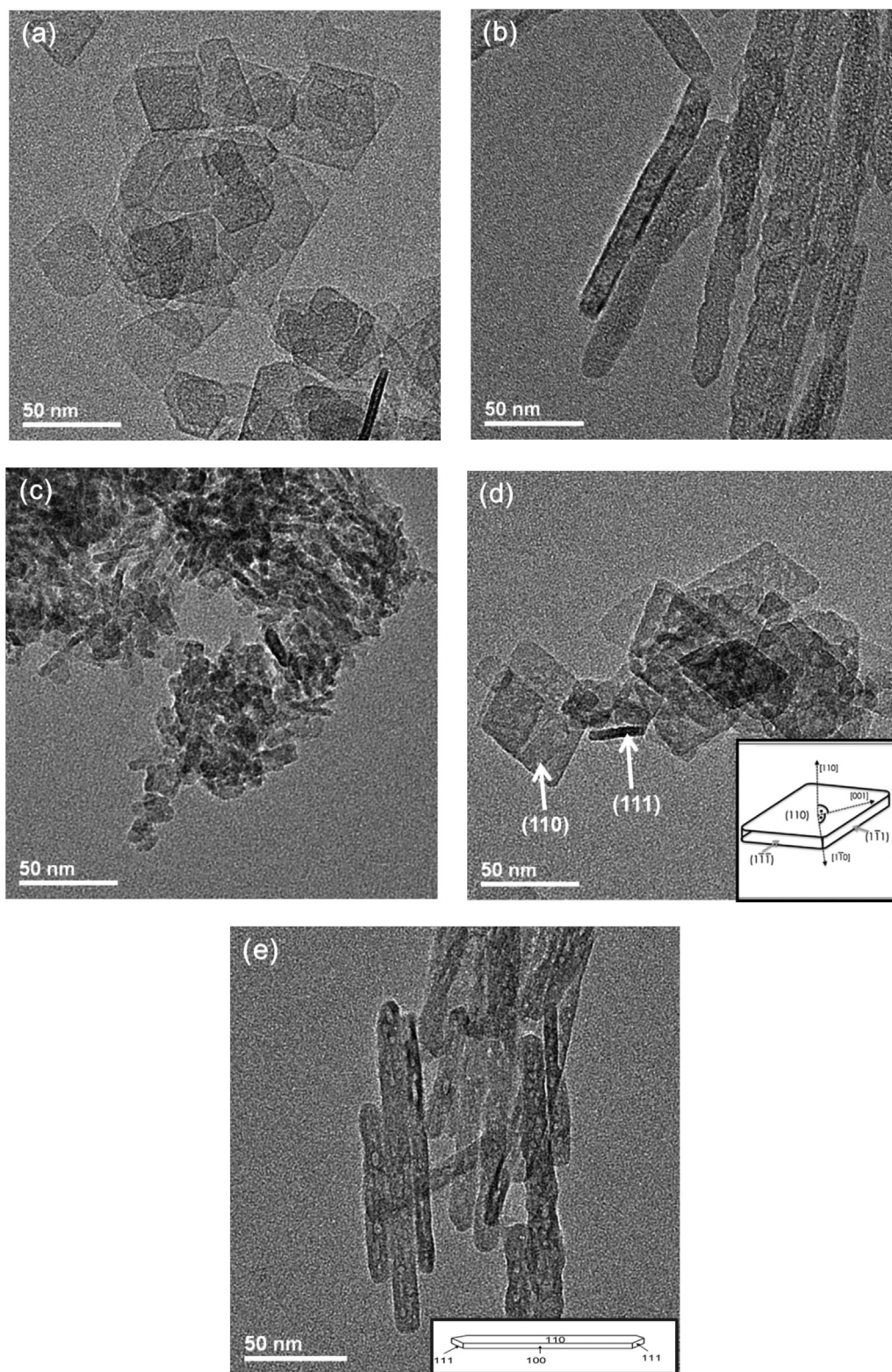
Fig. 2. TEM images for platelet (a), rod (b) boehmites and commercial (c), platelets (d) and rods (e) γ-Al$_2$O$_3$. (d) and (e) These are TEM images after calcination at 600 °C of (a) and (b). (Inset shows the indexing of the crystallographic planes and directions in terms of a cubic crystal lattice [2,22]).

Fig. 4(b). After 900 °C calcination, the δ-phase was detected with somewhat sharper peaks than those in the commercial alumina that can originate from the larger crystalline domain size of this sample. After 1000 °C treatment, new diffraction peaks at 31.8°, 32.9°, 51.1°, and 60.3° corresponding to θ-Al$_2$O$_3$ phase developed

[31,33], indicating the presence of a mixed δ/θ phase. After 1100 °C treatment, the intensities of the θ-Al$_2$O$_3$ related peaks increased significantly. The XRD pattern obtained from platelet alumina after 1100 °C treatments were very similar to the θ-Al$_2$O$_3$ reported by Zhoe and Snyder [33]. The highly crystalline platelet alumina after
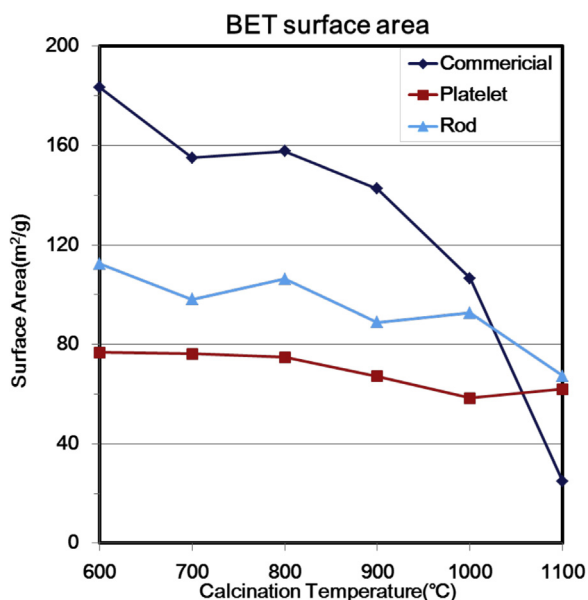
Fig. 3. BET surface area changes of aluminas after calcination at specific temperature for 3 h.

Table 1
The number of chemisorbed ethanol/nm^2 of alumina surface on commercial-, platelet- and rod-aluminas as a function of activation temperature.

Calcination temperature (°C)	Dissociative adsorption (ethanol/nm^2)		
	Commercial	Platelet	Rod
600	1.3	1.8	1.6
700	1.6	1.8	1.6
800	1.5	1.7	1.3
900	1.3	1.6	1.8
1000	1.2	1.4	1.4
1100	0.6	0.9	1.2

1100 °C calcination suggests relatively more pure θ-phase than before which might be expected to give insights for structural information of θ-Al_2O_3 [34]. Fig. 4(c) shows XRD patterns of rod-shaped alumina. At 900 °C rod-shaped alumina showed δ-Al_2O_3 phase but slightly different pattern from both commercial and platelet aluminas as the diffraction peak at $2\theta = 33°$ showed higher intensity in these latter samples. Here, rod-shaped alumina displayed narrower peaks and higher intensities at 30° than 33°. In the 1000–1100 °C temperature region, the intensities of diffraction peaks at 2θ values of 31.8°, 32.9°, 51.1°, and 60.3°, corresponding to θ-Al_2O_3 phase, increased [31]. Especially, it showed different XRD patterns from both commercial and platelet aluminas discussed above. After 1000 °C and 1100 °C calcinations, rod-shaped alumina systematically showed higher intensities of the peak at $2\theta = 30°$ than the peak at 33°. However, platelet alumina showed much higher intensities at $2\theta = 33°$ than 30°. Also, in 2θ region of 44–48°, the 1100 °C calcined rod-shaped alumina showed different XRD patterns from platelet alumina treated under identical conditions. Rod-shaped alumina showed only two peaks at 2θ values of 44.7° and 47.7°. This pattern is different from the platelet-shaped alumina which showed four peaks at $2\theta = 44.7°$, 45.5°, 46.5°, and 47.7°. These different XRD patterns suggest different structural evolution for the platelet- and rod-shaped aluminas upon calcination. Consistent with previous reports, the platelet shaped γ-alumina transformed into θ-phase, while rod-shaped alumina transformed to a phase similar to δ-Al_2O_3 [31,33].

Although XRD is the most commonly used bulk analysis technique to determine the phases of crystalline materials, it is ineffective for detecting changes in surface structures which might be different from the bulk. Chemical probes, on the other hand, are ideally suited to provide information about surface properties of solids. Ethanol TPD has shown remarkable sensitivity toward the surface structures of aluminas [18,30]. In our prior work we investigated ethanol TPD to verify the modification of surface characteristics of a commercial alumina sample by high temperature treatment. Before ethanol adsorption all samples were calcined at 500 °C to ensure the dehydration/dehydroxylation of alumina surfaces [30].

Fig. 5 shows the ethanol desorption profiles obtained for the three alumina samples studied in this work. Each ethanol TPD trace showed two peaks: one below 150 °C, which related to molecularly

adsorbed ethanol and another one above 200 °C originating from dissociatively adsorbed ethanol. These TPD profiles were similar to previously reported profiles for aluminas [30].

Here we are only interested in the change in the high temperature desorption profiles which showed direct correlation with changes in the alumina surface structure during phase transformations [18].

The three alumina samples showed the same trend: the maximum ethanol desorption temperature shifted to higher values with increasing calcination temperature. On commercial alumina (Fig. 5(a)), the desorption peak temperature after the 600 °C calcinations appeared at 247 °C and shifted to 267 °C, 277 °C, finally 367 °C after 3 h calcination at 900 °C, 1000 °C, and 1100 °C, respectively. For platelet alumina (Fig. 5(b)), after 600 °C thermal treatment, this peak appeared at 247 °C identical to that on commercial alumina. Upon high temperature calcinations this peak shifted gradually to 264 °C, 277 °C, and 327 °C for the 900 °C, 1000 °C and 1100 °C calcined samples, respectively. For rod-shaped alumina (Fig. 5(c)), the desorption peak shifted from 241 °C to 252 °C, 267 °C, and finally 292 °C after the same thermal treatment.

The commercial and platelet alumina samples showed exactly the same ethanol desorption temperatures at 247 °C before high temperature treatments. This result suggests that these two alumina samples have very similar surface characteristics, even though their morphologies were fundamentally different. The slightly lower desorption temperature (241 °C) observed for the rod-shaped alumina might be related to the very different facet ratio of this sample from the other two alumina samples. Desorption amounts decreased with calcination temperature, consistent with the overall decrease of surface areas determined by the BET method. For more quantitative information, we calibrated the amount of desorbed ethanol and normalized based on alumina surface area. The results summarized in Table 1. All samples basically demonstrate the same trend: chemisorbed ethanol amount shows maximum at around 700 °C then decreases with calcination temperature. These results are consistent with the two factors affecting the chemisorption of ethanol that the surface dehydroxylation which will increase with activation temperatures and that the alumina phase transformations which starts at around 700 °C.

The TPD peak positions for the 900 °C calcined alumina samples were different for the three samples of different morphologies. Commercial alumina showed a peak at 267 °C, while the platelet- and rod-shaped aluminas exhibited desorption features at 264 °C and 252 °C, respectively. After 1100 °C calcination the TPD peak positions of the three alumina samples, shown in Fig. 5(d), were also significantly different. In the TPD profile of the commercial Al_2O_3 the peak appeared at 367 °C, while for the platelet- and rod-shaped alumina samples this high temperature desorption feature was centered at 327 °C and at 292 °C, respectively. The different desorption temperatures observed for aluminas calcined under identical conditions suggest that their surface characteristics changed differently during thermal processing. These results are consistent with the data of XRD analysis that revealed morphology-dependent
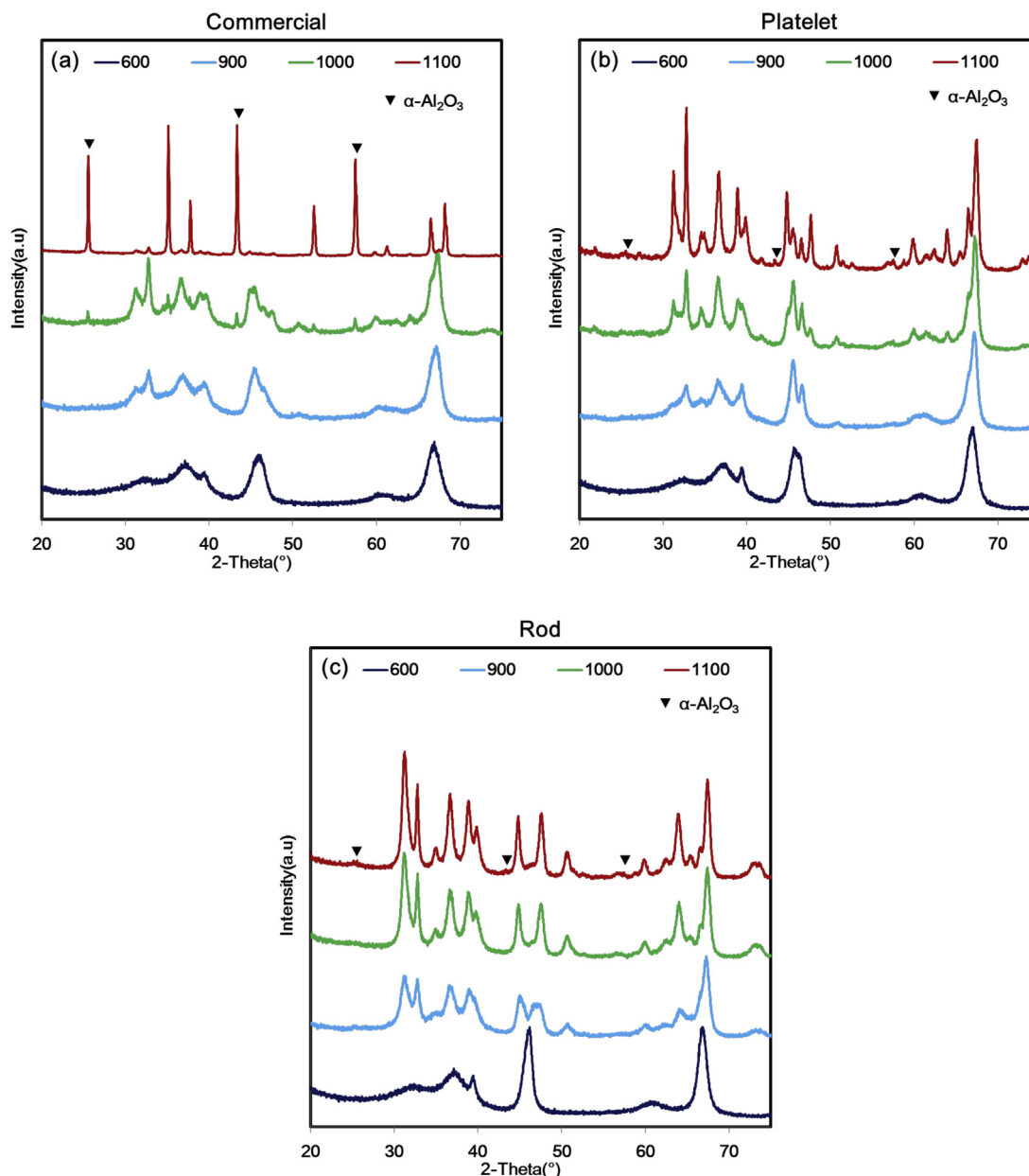
Fig. 4. XRD patterns for thermo-treated alumina samples at selected temperatures (600 °C, 900 °C, 1000 °C, and 1100 °C). (a) Commercial, (b) platelets, and (c) rods. The solid triangles are given as guides to the α-phase.

phase transformation for these three alumina samples. Combining the results of ethanol TPD and XRD (i.e., a surface and a bulk technique) allows us to conclude that not only the bulk phase but the surface characteristics of these three γ-Al_2O_3 samples changed differently during identical calcination procedures. Especially, the maximum ethanol desorption temperature changes in the order of commercial > platelet > rod-shaped alumina. It is also consistent with XRD results that, after 1100 °C treatment, the commercial γ-Al_2O_3 transformed into α-phase while platelet- and rod-shaped aluminas did not transform to α-Al_2O_3.

Beside variation in the temperature of maximum desorption rate, the TPD traces of Fig. 5(d) clearly demonstrate that the amount of desorbed ethanol also changes with alumina preparation. Platelet- and rod-shaped aluminas showed significantly higher amounts of desorption products than the commercial alumina after the 1100 °C calcinations. The small area of high temperature desorption peak from commercial alumina is most

probably related to its small surface area (25 m^2/g). Interestingly, the integrated area under the high temperature desorption peak of rod-shaped alumina was almost twice as high as that of the platelet alumina, despite their very similar surface areas (62 m^2/g for platelet and 67 m^2/g for rod-shaped aluminas). These results suggest that the sites where dissociative ethanol adsorption takes place are related to some specific facets of the alumina surface. The ratio of these facets is significantly different due to clearly different morphologies despite their similar surface areas. These drastic changes of ethanol desorption amount with desorption temperature will affect the ethanol dehydration reaction on these three types of alumina samples.

In order to understand the changes in the morphologies of these different aluminas during thermal treatment [10,21], TEM images were collected for the calcined samples and displayed in Fig. 6. Fig. 6(a) demonstrates the morphological change of commercial alumina by high temperature treatment. After 1100 °C calcination,
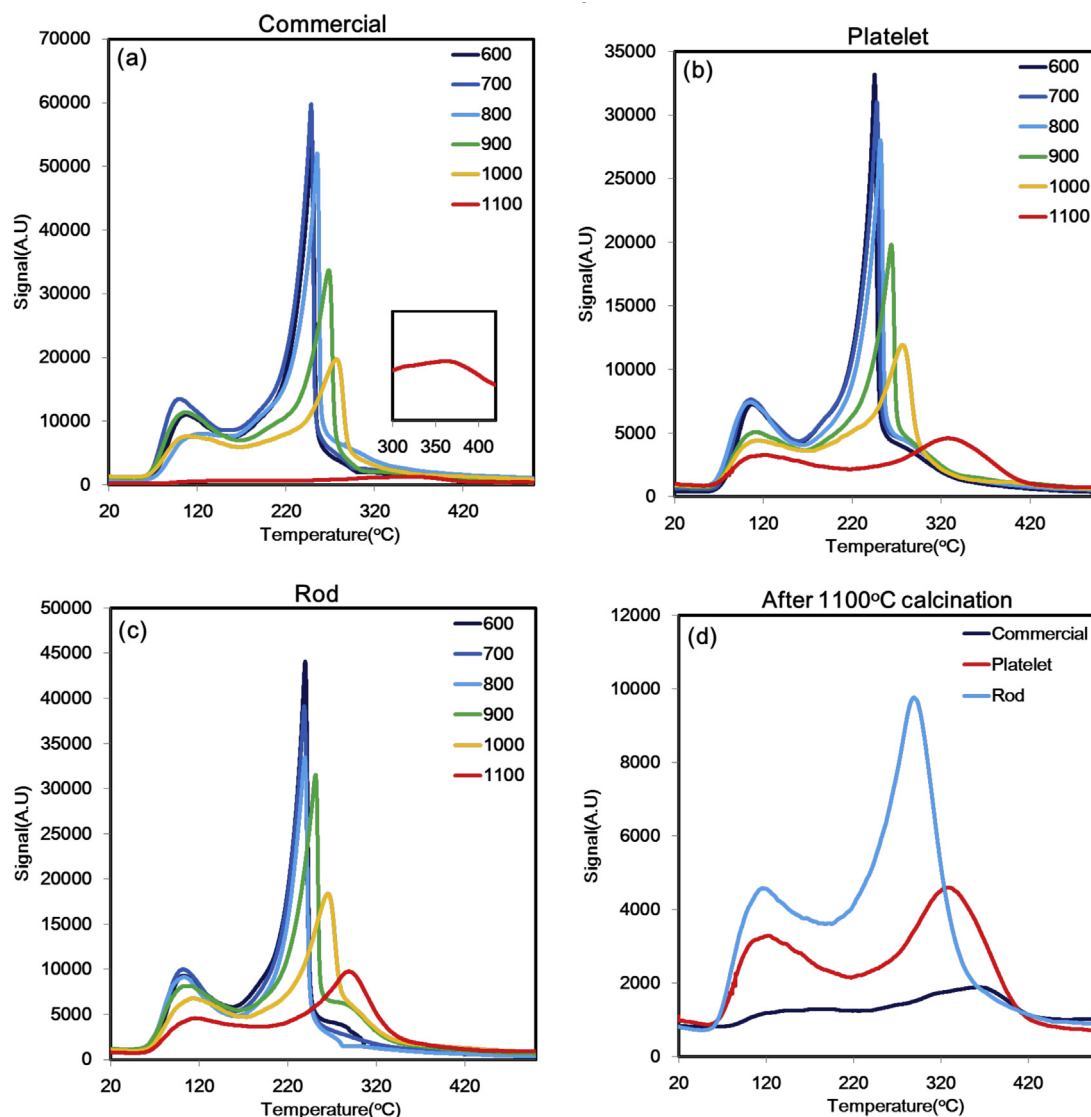
Fig. 5. Ethanol TPD profiles on alumina samples calcined at the indicated temperature. (a) Commercial (inset: ethanol-TPD on 1100 °C calcined sample), (b) platelets, (c) rods, and (d) ethanol TPD profiles for the 1100 °C-calcined samples.

large agglomerates with completely different morphology from the original commercial alumina were observed. The agglomeration of small crystallites of the original commercial alumina to large α-Al_2O_3 crystals is evident, and it appears that the small crystals were fused together to form the large ones. On the contrary, both platelet- and rod-shaped aluminas retained their original morphological shapes even after 1100 °C calcination.

Fig. 6(b) shows that the well-defined platelets with rhombus shapes were maintained after calcination at 600 °C and even at 900 °C. The platelets after the 1100 °C calcination maintained their overall rhombus shape, however, some distortions appeared at the edges of these crystallites. The TEM images presented in Fig. 6(c) for the rod-shaped alumina sample reveal that no apparent morphological change took place during high temperature calcinations up to 1100 °C. Unlike the platelets which exhibited some distortions after the highest temperature calcinations, the rod-shaped crystallites showed no apparent surface distortion. On TEM measurement, both 1100 °C calcined platelet and rod alumina showed high crystallinity which is also consistent with the sharp XRD diffraction pattern recorded after the 1100 °C calcination. These results are consistent with the improved thermal stability of

platelet- and rod-shaped aluminas compared with the commercial alumina.

During phase transitions of γ-Al_2O_3 significant modifications in the environment of Al^{3+} ions in the crystal lattice and on the surface facets can be expected. ^{27}Al-NMR provides us an excellent opportunity to follow the changes in the coordination environments of the Al^{3+} ions [9,17]. Fig. 7(a) shows ^{27}Al-MAS-NMR spectra for the commercial alumina sample after calcinations at selected temperatures (600 °C, 1000 °C, and 1100 °C). The ^{27}Al-MAS-NMR spectrum of the 600 °C-calcined commercial γ-Al_2O_3 substantiate the presence of both octahedral and tetrahedral Al^{3+} ions as it is manifested by the peaks observed ~13 ppm and ~72 ppm chemical shifts, respectively (typical γ-Al_2O_3 spectrum reported previously) [17]. After 1000 °C calcination, the amount of tetrahedral Al^{3+} increased from 35% to 37% (the percentage of the total number of Al^{3+} ions). After thermal treatment at 1100 °C for 3 h, the octahedral Al^{3+} peak shifted to ~16 ppm and its intensity increased significantly, strongly supporting the extensive formation of the α-Al_2O_3 phase [35]. However, some residual tetrahedral Al^{3+} are also detected, suggesting the presence of some other phases in this sample (most probably θ-phase). This finding is consistent with those
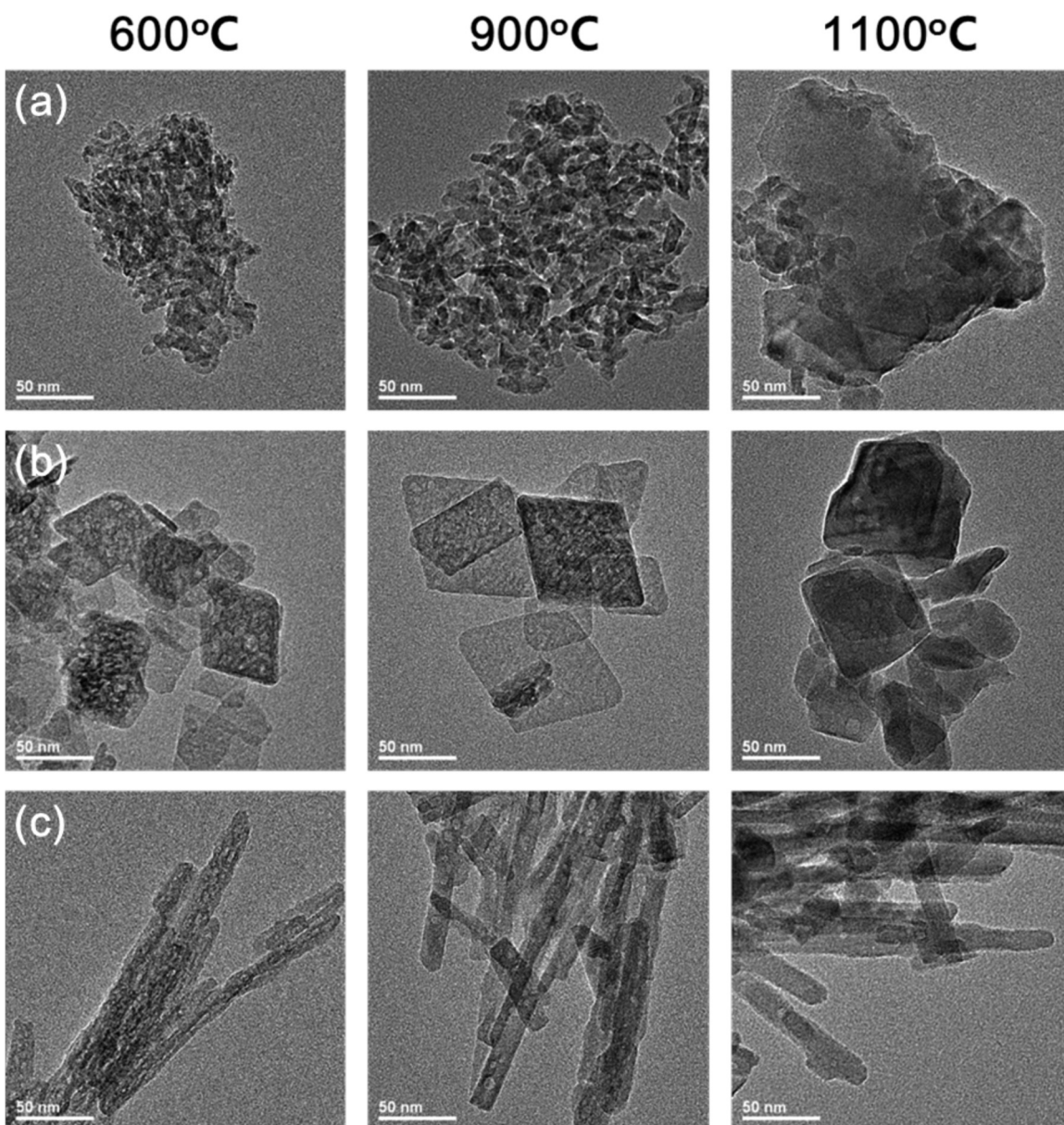
Fig. 6. TEM images for the thermally treated alumina samples in low magnification (a) commercial, (b) platelets, and (c) rods at 600 °C, 900 °C, and 1100 °C.

deduced from the XRD pattern where, beside the majority of peak characteristic of the α-Al$_2$O$_3$ phase, other peaks belonging to other alumina phases (in particular θ) remained with very low intensity.

Fig. 7(b) shows ^{27}Al-MAS-NMR spectra for the platelet alumina sample calcined under the same conditions as the commercial alumina. The 600 °C-calcined sample exhibits an octahedral peak at ~13 ppm and tetrahedral peak at ~72 ppm chemical shifts. After 1000 °C heat treatment, the octahedral Al^{3+} peak shifted to ~9 ppm and became much sharper than that obtained from 600 °C-calcined sample, suggesting a more uniform chemical environment of the Al^{3+} ions in this calcined sample. At the same time, the peak of the tetrahedral Al^{3+} ions develops a shoulder at ~78 ppm. These results are interpreted as a consequence of phase transformation from γ- to δ- and/or θ-Al$_2$O$_3$ during high temperature treatment. After 1100 °C calcination, the octahedral Al^{3+} peak remains unchanged, while the intensity of the tetrahedral Al^{3+} peak increases significantly. In this sample the ratio between tetrahedral and octahedral sites is 0.44:0.56, consistent with previous reports showing that the tetrahedral and octahedral Al^{3+} ratio is 1:1 for the ideal θ-Al$_2$O$_3$

[9]. If we consider the presence of very low intensity of XRD peaks associated with the α-Al$_2$O$_3$ phase (octahedral aluminum only) at $2\theta = 25.7°$, $43.4°$, and $57.6°$, the tetrahedral vs. octahedral aluminum ratio is very close to 1:1 in this platelet shaped alumina sample. The interesting line shapes of tetrahedral aluminum ions are related with the chemical environment of tetrahedral Al^{3+} in θ-Al$_2$O$_3$ unit cells. By combining XRD peaks showing high crystalline θ-Al$_2$O$_3$ phase and tetrahedral vs. octahedral Al^{3+} ratio from NMR spectrum, further studies of platelet alumina after 1100 °C are expected to give insights on the structural information of θ-Al$_2$O$_3$ [34].

Fig. 7(c) displays ^{27}Al-MAS-NMR spectra obtained from the rod-shaped alumina samples after calcinations at different temperature. The ^{27}Al-MAS-NMR spectrum of the 600 °C-calcined, rod-shaped alumina sample is practically identical to that of the commercial and platelet-shaped γ-Al$_2$O$_3$. After 1000 °C treatment, it exhibits very similar spectrum to that of platelet-shaped Al$_2$O$_3$. The 1100 °C calcined rod-shaped Al$_2$O$_3$ shows a high intensity NMR peak of tetrahedral Al^{3+} sites and the observed line shapes can be related to δ-Al$_2$O$_3$ (we could not find significant
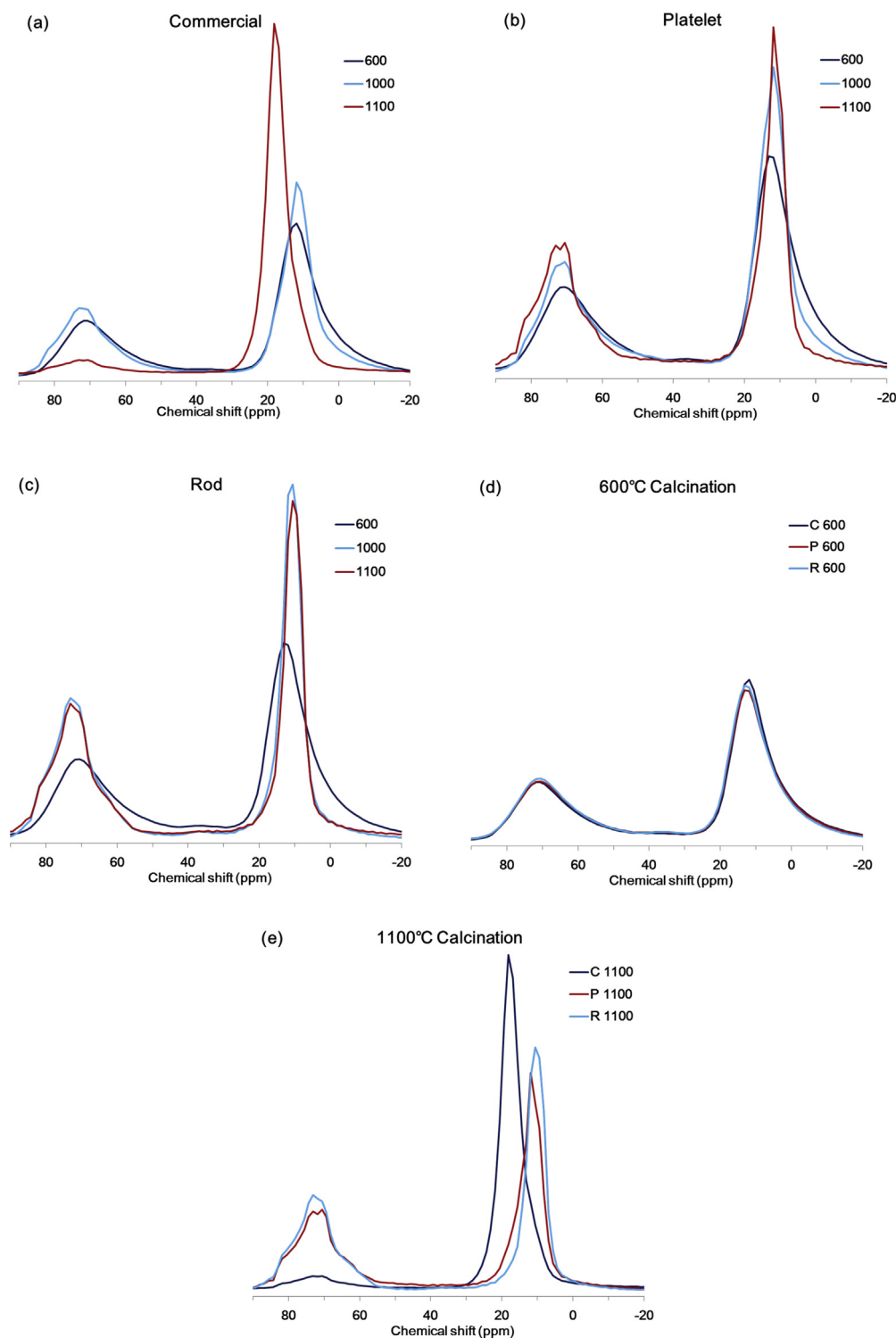
Fig. 7. Solid state ^{27}Al-MAS-NMR spectra for the thermally treated (a) commercial, (b) platelet- and (c) rod-shaped γ-Al$_2$O$_3$ after 600 °C, 1000 °C, and 1100 °C calcination. Solid state ^{27}Al-MAS-NMR spectrum for (d) 600 °C and (e) 1100 °C calcined samples.

difference between θ-Al$_2$O$_3$ phases formed from platelet- and rod-shaped aluminas). The octahedral aluminum peak located at ~10 ppm suggests that the rod-shaped alumina does not produce significant amount of α-Al$_2$O$_3$ that shows an octahedral aluminum peak at ~16 ppm. And the remaining tetrahedral Al^{3+} is also consistent with XRD results showing very minor α-Al$_2$O$_3$ formation. The intensity ratio between tetrahedral and octahedral Al^{3+} sites is 0.45:0.55, similar to that in platelet

Al$_2$O$_3$ after 1100 °C thermal treatment. In contrast, the XRD pattern of the rod-shaped alumina sample is very different from that of the platelet Al$_2$O$_3$, suggesting that they indeed proceed through different crystallization (phase transformation) paths. Additional detailed studies for platelet- and rod-shaped Al$_2$O$_3$ phases formed after high temperature treatments are required to fully understand the processes occurring during high temperature calcinations.
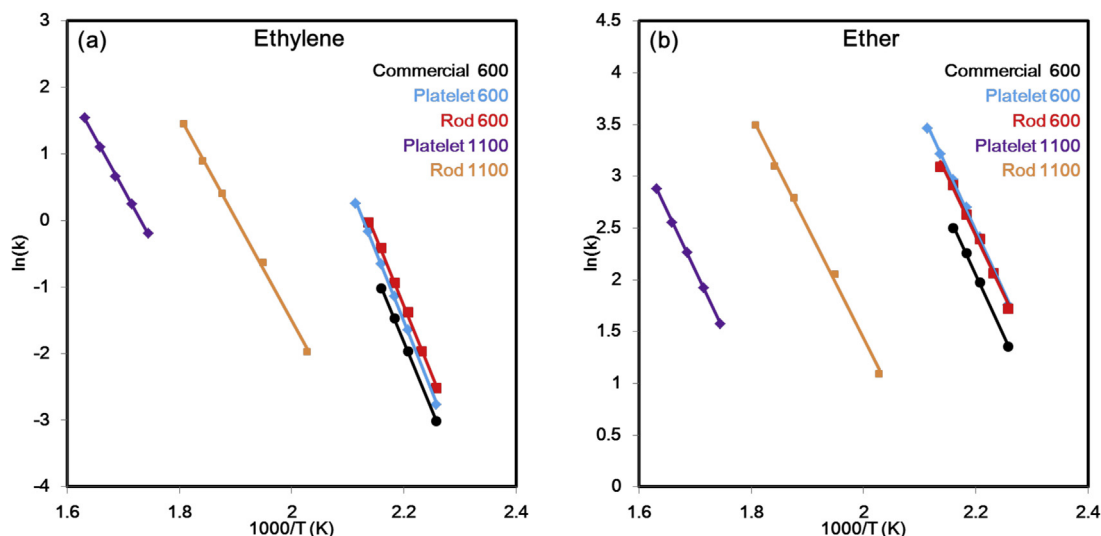
Fig. 8. Ethanol dehydration activity over commercial, platelet- and rod-shaped aluminas after calcination at 600 °C and 1100 °C ((a) ethylene and (b) diethyl ether). The ethanol dehydration reaction temperatures were from 170 °C and 200 °C for 600 °C calcined alumina, 220–280 °C for 1100 °C calcined rod-shaped alumina and 300–340 °C for 1100 °C calcined platelet-shaped alumina.

For easy comparison, Fig. 7(d) and (e) show ^{27}Al-MAS-NMR spectra for aluminas thermally calcined at 600 °C and 1100 °C. At 600 °C, commercial, platelet and rod all consistently showed identical NMR spectra. All showed two main peaks at 13 ppm and 72 ppm, which is typically γ-Al_2O_3. However, at 1100 °C explicit difference appeared on tetrahedral Al^{3+} peak. Commercial showed drastically reduced intensity while platelet and rod aluminas remained their tetrahedral Al^{3+} sites peak intensities. On octahedral Al^{3+}, commercial alumina showed high intensity peak at 16 ppm suggesting α-Al_2O_3. Platelet and rod Al_2O_3 showed no peak at 16 ppm which suggests that both did not transform to α-Al_2O_3.

The results of ethanol TPD experiments discussed above suggested that the 1100 °C treated Al_2O_3 samples may exhibit different catalytic behavior for ethanol dehydration [36–41]. To this end, we carried out ethanol dehydration experiments on both 600 °C and 1100 °C calcined Al_2O_3 samples, which showed apparent differences in ethanol TPD.

Fig. 8 shows ethanol dehydration activities measured on selected alumina samples. For easy comparison, we normalized the ethanol dehydration activity based on the surface area of alumina. Interestingly, within experimental error, all three 600 °C-calcined γ-Al_2O_3 samples showed very similar ethanol dehydration activities and selectivities, despite their very different morphologies. This might be related to the same γ-Al_2O_3 structure and very similar surface characteristics attested by ethanol TPD, even though their morphologies are different. Activation energies calculated for ethylene and di-ethyl ether production were 170–175 kJ/mol and 95–98 kJ/mol, respectively (Table 1).

The ethanol dehydration activities of the 1100 °C-calcined alumina samples decreased significantly. For commercial Al_2O_3, the activity was very low although ethanol dehydration was carried out up to 300 °C. This is, at least partly, the consequence of very low (25 m^2/g) surface area of the commercial Al_2O_3 sample after it phase-transformed to α-Al_2O_3. In ethanol TPD this sample showed very small desorption amount in the high temperature desorption state. Therefore, it seems reasonable to associate the low activity observed in the 1100 °C-calcined sample to the small amount of strongly bound ethanol on α-Al_2O_3 surfaces. Ethanol dehydration reaction activities of the other two aluminas (platelet- and rod-shaped) after 1100 °C calcination were also very low in comparison to the original γ-Al_2O_3. When we compare the high temperature activities of these alumina samples calcined at 1100 °C, we found that at same reaction temperature the rod-shaped alumina showed much higher ethanol dehydration activity than platelet alumina (Fig. 8). This observation seems to correlate well with ethanol TPD profiles of the 1100 °C treated alumina samples presented above. Although the BET surface areas were very similar on these two samples, they exhibited different ethanol desorption amounts and maximum desorption rate temperatures. In light of these results it is reasonable to assume that relatively high desorption amount and lower desorption temperature on rod-shaped alumina translates into higher catalytic activity in comparison to the platelet alumina. Interestingly, the activation energy for ethylene formation decreased from 170–175 kJ/mol (on γ-Al_2O_3) to 126–127 kJ/mol for both platelet and rod shaped aluminas. On the contrary, the activation energy for diethyl ether formation was 89–94 kJ/mol for all three γ-Al_2O_3 samples (Table 1). These results suggest a potential change in reaction mechanism or active sites between ethylene and diethyl ether. Detailed understanding of ethanol dehydration and activation energies will require further studies. In this study, we only focused on how the variation in crystallite morphologies affected both the phase transformation and the surface chemistry (as probed by ethanol TPD and ethanol reaction) of Al_2O_3 (Table 2).

Table 2
Conversion, selectivity, and activation energy for the ethanol dehydration reaction over selected aluminas.

Sample	Calcination temperature (°C)	Reaction temperature (°C)	Conversion (%)	Selectivity		Activation energy	
				$S_{ethylene}$ (%)	S_{ether} (%)	Ethylene (kJ/mol)	Ether (kJ/mol)
Commercial	600	180	4.59	1.91	98.1	170.5	98.5
Platelet	600	180	2.98	1.69	98.3	175.7	98.5
Rod	600	180	3.06	2.25	97.7	172.8	95.0
Platelet	1100	300	1.25	13.8	81.3	126.6	94.8
Rod	1100	260	4.07	8.42	91.5	127.4	89.2

4. Conclusions

In this work, we investigated the phase transformation of platelet- and rod-shaped γ-Al_2O_3 by XRD, BET, HR-TEM, solid state ^{27}Al-NMR, and ethanol TPD after sequential annealing in air up to 1100 °C and compared them with a commercial. After annealing at 1100 °C, commercial γ-Al_2O_3 transformed to α-Al_2O_3 with drastic surface area reduction (initially 200 m^2/g to 25 m^2/g after 1100 °C treatment). Interestingly, platelet- and rod-shaped aluminas which showed exactly same initial XRD patterns transformed into different phases. Platelet-shaped γ-Al_2O_3 transformed mostly to θ-Al_2O_3, while rod-shaped γ-Al_2O_3 phase transformed preferentially to δ-Al_2O_3. Both aluminas sustained significantly higher surface area ($\sim$60 m^2/g) than the commercial one under identical conditions. These results strongly suggest that the phase transformation of γ-Al_2O_3 is strongly affected by not only the elementary crystalline structure of the starting materials, but also by their secondary morphologies.

Ethanol TPD traces collected from platelet- and rod-shaped aluminas after 1100 °C annealing showed significantly different desorption profiles which suggest different surface characteristics, although their surface areas remained very similar. These different phase transformations were also supported by solid state ^{27}Al-NMR. Commercial alumina shows mostly octahedral Al^{3+} ions after 1100 °C annealing, consistent with the formation of the α-phase, but the other two samples show even higher intensities of tetrahedral Al^{3+} ions than the initial γ-Al_2O_3 does. Morphological changes were also confirmed by TEM. Surface distortion appeared in the 1100 °C-calcined platelets, but no apparent change was seen in the rod-shaped alumina. Also, 1100 °C calcined alumina showed different catalytic behavior for ethanol dehydration which was consistently supported by ethanol TPD. After 1100 °C calcinations the order of ethanol dehydration activity was rod > platelet > commercial alumina. These results consistently suggest the morphology-dependent phase transformations of γ-Al_2O_3 and improved thermal stability of platelet- and rod-shaped γ-Al_2O_3 in comparison to a commercial γ-Al_2O_3 only by morphological change without any surface modifiers.

Finally, nano-faceted Al_2O_3 with well-defined morphologies (platelet and rod) are ideally good model system which might enable the fundamental study how the metal interacts with Al_2O_3 in atomic level otherwise difficult with commercial Al_2O_3 [34,42,43]. This study gives insights into surface characteristic change on these well-defined model systems.

Acknowledgments

References

[1] I. Levin, D. Brandon, J. Am. Ceram. Soc. 81 (1998) 1995–2012.
[2] G. Busca, Catal. Today 226 (2014) 2–13.
[3] M. Trueba, S.P. Trasatti, Eur. J. Inorg. Chem. 17 (2005) 3393–3403.
[4] P. Eklund, M. Sridharan, G. Singh, J. BØttiger, Plasma Process. Polym. 6 (2009) 907–911.
[5] V. Edlmayr, T.P. Harzer, R. Hoffmann, D. Kiener, C. Scheu, C. Mitterer, J. Vac. Sci. Technol. A 29 (2011) 041506.
[6] K. Bobzin, N. Bagcivan, A. Reinholdt, M. Ewering, Surf. Coat. Technol. 205 (2010) 1444–1448.
[7] J. Musil, J. Blazek, P. Zeman, S. Proksova, M. Sasek, R. Cerstvy, Appl. Surf. Sci. 257 (2010) 1058–1062.
[8] P. Nayar, A. Khanna, D. Kabiraj, S.R. Abhilash, B.D. Beake, Y. Losset, B. Chen, Thin Solid Films 568 (2014) 19–24.
[9] C. Pecharroman, I. Sobrados, J.E. Iglesias, T. Gonzalez-Carreno, J. Sanz, J. Phys. Chem. B 103 (1999) 6160–6170.
[10] P.S. Santos, H.S. Santos, S.P. Toledo, Mater. Res. 3 (2000) 104–114.
[11] M. Machida, K. Eguchi, H. Arai, J. Catal. 103 (1987) 385–393.
[12] R.N. Das, A. Hattori, K. Okada, Appl. Catal. A 207 (2001) 95–102.
[13] M. Ozawa, Y. Nishio, J. Alloys Compd. 374 (2004) 397–400.
[14] S.W. Wang, A.Y. Borisevich, S.N. Rashkeev, M.V. Glazoff, K. Sohlberg, S.J. Pennycook, S.T. Pantelides, Nat. Mater. 3 (2004) 143–146.
[15] I. Balint, Z. You, K. Aika, Phys. Chem. Chem. Phys. 4 (2002) 2501–2503.
[16] R.H.R. Castro, S.V. Ushakov, L. Genermbre, D. Gouvea, A. Novrotsky, Chem. Mater. 18 (2006) 1867–1872.
[17] J.H. Kwak, J. Hu, A. Lukaski, D.H. Kim, J. Szanyi, C.H.F. Peden, J. Phys. Chem. C 112 (2008) 9486–9492.
[18] J.H. Kwak, C.H.F. Peden, J. Szanyi, J. Phys. Chem. C 115 (2011) 12575–12579.
[19] N. Lepot, M.K.V. Bael, H.V.D. Rul, J. D'Haen, R. Peeters, D. Franco, J. Mullens, Ceram. Int. 34 (2008) 1971–1974.
[20] M.G. Ma, Y.J. Zhu, Z.L. Xu, Mater. Lett. 61 (2007) 1812–1815.
[21] X.Y. Chen, Z.J. Zhang, X.L. Li, S.W. Lee, Solid State Commun. 145 (2008) 368–373.
[22] P.D.S. Santos, A.C.V. Coelho, H.D.S. Santos, P.K. Kiyohara, Mater. Res. 12 (2009) 437–445.
[23] Y. Mathieu, B. Lebeau, V. Valtchev, Langmuir 23 (2007) 9435–9442.
[24] Y. Xia, X. Jiao, Y. Liu, D. Chen, L. Zhang, Z. Qin, J. Phys. Chem. C 117 (2013) 15279–15286.
[25] T. He, L. Xiang, S. Zhu, CrystEngComm 11 (2009) 1338–1342.
[26] M. Konsolakis, N. Macleod, J. Isaac, I.V. Yentekakis, R.M. Lambert, J. Catal. 193 (2000) 330–337.
[27] G. Avgouropoulos, E. Oikonomopoulos, D. Kanistras, T. Ioannides, Appl. Catal. B 65 (2006) 62–69.
[28] C. Mager-Maury, C. Chizallet, P. Sautet, P. Raybaud, ACS Catal. 2 (2012) 1346–1357.
[29] H. Shi, O.Y. Gutiérrez, H. Yang, N.D. Browning, G.L. Haller, J.A. Lercher, ACS Catal. 3 (2013) 328–338.
[30] J.H. Kwak, D. Mei, C.H.F. Peden, R. Rousseau, J. Szanyi, Catal. Lett. 141 (2011) 649–655.
[31] M. Nguefack, A.F. Popa, S. Rossignol, C. Kappenstein, Phys. Chem. Chem. Phys. 5 (2003) 4279–4289.
[32] M. Digne, P. Sautet, P. Raybaud, P. Euzen, H. Toulhoat, J. Catal. 226 (2004) 54–68.
[33] R.S. Zhou, R.L. Synder, Acta Crystallogr. B47 (1991) 617–630.
[34] L. Kovarik, M. Bowden, A. Genc, J. Szanyi, C.H.F. Peden, J.H. Kwak, J. Phys. Chem. C 118 (2014) 18051–18058.
[35] J.J. Fitzgerald, G. Piedra, S.F. Dec, M. Seger, G.E. Maciel, J. Am. Chem. Soc. 119 (1997) 7832–7842.
[36] H. Knözinger, Angew. Chem. Int. Ed. 7 (1968) 791–805.
[37] S. Roy, G. Mpourmpakis, D.Y. Hong, D.G. Vlachos, A. Bhan, R.J. Gorte, ACS Catal. 2 (2012) 1846–1853.
[38] M.A. Christiansen, G. Mpourmpakis, D.G. Vlachos, ACS Catal. 3 (2013) 1965–1975.
[39] J.F. DeWilde, H. Chiang, D.A. Hickman, C.R. Ho, A. Bhan, ACS Catal. 3 (2013) 798–807.
[40] T.K. Phung, A. Lagazzo, M.A. Rivero Crespo, V. Sanchez Escribano, G. Busca, J. Catal. 311 (2014) 102–114.
[41] J.F. DeWilde, C.J. Czopinski, A. Bhan, ACS Catal. 4 (2014) 4425–4433.
[42] L. Kovarik, A. Genc, C. Wang, A. Qiu, C.H.F. Peden, J. Szanyi, J.H. Kwak, J. Phys. Chem. C 117 (2013) 179–186.
[43] L. Roiban, L. Sorbier, C. Pichon, C. Pham-Huu, M. Drillon, O. Ersen, Nanoscale 4 (2012) 946–954.